Available online at www.sciencedirect.com
SCIENCE DIRECT®
International Journal of Heat and Mass Transfer 48 (2005) 4397–4409
International Journal of HEAT and MASS TRANSFER
www.elsevier.com/locate/ijhmt

Flow pattern transition instability in a microchannel with CO_2 bubbles produced by chemical reactions

B.R. Fu, Chin Pan *

Department of Engineering and System Science, National Tsing Hua University, Hsinchu, 30043 Taiwan, ROC

Received 18 March 2005; received in revised form 12 May 2005
Available online 19 July 2005

Abstract

The present study investigates experimentally the two-phase flow in a rectangular microchannel with CO_2 bubbles generated by chemical reactions of sulfuric acid (H_2SO_4) and sodium bicarbonate ($NaHCO_3$). The microchannel with a hydraulic diameter of 132.7 μm is prepared using bulk micromachining and anodic bonding process. Evolution of two-phase flow patterns in the microchannel was observed using a high speed video camera and the corresponding pressure drop was investigated. It is found that the inlet concentration and flow rate of reactants have a significant effect on the evolution of two-phase flow characteristics and slug flow is the dominant flow pattern. The flow pattern transition instability between bubbly-slug and slug flow takes place for the cases with highest inlet concentration, i.e., $C = 0.8$ mol/L, and low flow rates of this study. The oscillation frequency is from 0.024 to 0.041 Hz and the magnitude of oscillation in pressure drop is from 10 to 15 kPa. A mechanism based on the flow circulation in the liquid slug may reasonably explain the flow pattern transition instability. Small amplitude, high frequency oscillations with a frequency of about 45 Hz are superimposed on the low frequency flow pattern transition as well as prevail for other cases without the flow pattern transition instability. The two-phase flow pressure drop increases with increase in both flow rate and inlet concentration.

Keywords: Flow pattern transition instability; Microchannel; Two-phase flow

1. Introduction

Micro direct methanol fuel cells (DMFCs) have shown good potential serving as power supplies for computer, communication and consumer electronics (3C) products because their high energy density. However, carbon dioxide is generated in the anode area due to the oxidation of methanol. The removal of CO_2 bubbles is of critical concern for the design of a micro DMFC. The CO_2 bubbles may result in the blockage of the micro fuel channel and significantly influence the performance of a micro DMFC [1]. Bubble departure from the channel wall is critical for the removal of CO_2 bubbles and Lee et al. [2] revealed that bubble departure in a uniform boiling microchannel is governed by the surface tension and the drag due to bulk two-phase flow. To study the bubble removal and simulate the two-phase flow phenomena in a micro fuel channel of a micro DMFC, Hwang et al. [3] explored the two-phase flow characteristics of ethanol/CO_2 in converging and diverging

* Corresponding author. Tel.: +886 3 5725363; fax: +886 3 5720724.
E-mail address: cpan@ess.nthu.edu.tw (C. Pan).

0017-9310/$ - see front matter © 2005 Elsevier Ltd. All rights reserved.
doi:10.1016/j.ijheatmasstransfer.2005.05.010

Nomenclature

A_1	cross-sectional area just before the expansion or after the contraction, (m^2)
A_{12}	A_1/A_2
A_2	cross-sectional area just before the contraction or after the expansion, (m^2)
C	mole concentration of reactant at the inlet before mixing, (mol/L)
D_H	hydraulic diameter of the microchannel, (m)
f	friction factor
L	length of the microchannel, (m)
Q_H	volume flow rate of sulfuric acid, (m^3/s)
Q_N	volume flow rate of sodium bicarbonate, (m^3/s)
Re	Reynolds number
V	velocity of fluid, (m/s)
$x_{H,\text{mole}}$	mole fraction of sulfuric acid in mixture solution
$x_{N,\text{mole}}$	mole fraction of sodium bicarbonate in mixture solution
$x_{H,\text{volume}}$	volume fraction of sulfuric acid in mixture solution
$x_{N,\text{volume}}$	volume fraction of sodium bicarbonate in mixture solution

Greek symbols

ΔP_{ex}	pressure loss at the outlet, (Pa)
ΔP_f	frictional pressure drop, (Pa)
ΔP_{in}	pressure loss at the inlet, (Pa)
ΔP_{total}	total pressure drop, (Pa)
γ	aspect ratio of the depth to the width of the channel
k	loss coefficient
μ_H	viscosity of sulfuric acid, (Pa s)
μ_{mix}	viscosity of mixture, (Pa s)
μ_N	viscosity of sodium bicarbonate, (Pa s)
ρ_H	density of sulfuric acid, (kg/m^3)
ρ_{mix}	density of mixture, (kg/m^3)
ρ_N	density of sodium bicarbonate, (kg/m^3)

microchannels with mean hydraulic diameters of 122 and 105 μm, respectively. Two-phase flow patterns and pressure drop in converging and diverging microchannels were investigated. They found that the acceleration effect and so the steep pressure gradient in a converging microchannel may result in the elongation of bubbles in slug flow, while the deceleration effect and so the possible pressure rise in the diverging microchannel causes shortening of bubbles in slug flow significantly. For both types of channel, the collision and merger of two consecutive bubbles may take place and result in twisting of bubbles.

The present study investigates experimentally the two-phase flow characteristics in a microchannel with CO_2 bubbles generated by chemical reactions of sulfuric acid and sodium bicarbonate

$$H_2SO_4 + 2NaHCO_3 \rightarrow Na_2SO_4 + 2H_2O + 2CO_2 \quad (1)$$

Meng et al. [4] employed the same chemical reaction to produce CO_2 bubbles in a stagnant system to study the removal of CO_2 bubbles. In the present work, the chemical reaction will take place in the microchannel while the reactant solutions flow through it and results in generation of CO_2 in the microchannel. Moreover, the corresponding two-phase flow drop through the channel are measured and analyzed under various different flow conditions and inlet concentrations. Such a bubble formation from chemical reactions in a microchannel may simulate more closely the transport phenomena of CO_2 bubbles in a micro DMFC than that of Hwang et al. [3].

Various different kinds of flow instability may take place in two-phase flow systems [5]. Two-phase flow instabilities have also been reported for flow boiling in microchannels, e.g. Li et al. [6], Wu and Cheng [7] and Qu and Mudawar [8]. Flow pattern transition instability is a kind of relaxation instability [5,9]. Although the flow pattern transition instability has been well-known, the primary mechanism for such instability in a microchannel with chemical reactions is still unexplored in the literature. Moreover, the flow rate in the present study remains constant for each case but the inlet pressure and thus the pressure drop is allowed to vary during the experiment. In the present work a kind of flow pattern transition instability is reported and its mechanism is explored.

2. Experimental detail

2.1. Experimental setup

A schematic diagram of the experimental setup, consisting of the test section, syringe pump, flow visualization system and pressure measurement system, is shown in Fig. 1. The syringe pump with two syringe tubes drove the two solutions (H_2SO_4 and $NaHCO_3$) simultaneously to the channel at the same flow rate. The exhausted fluids from the test section were drained to a container on an electronic balance, which might provide calibration of flow rate of each solution, one by one, before an experiment. Fig. 1 also shows the pressure tap locations at the inlet and outlet as shown. The

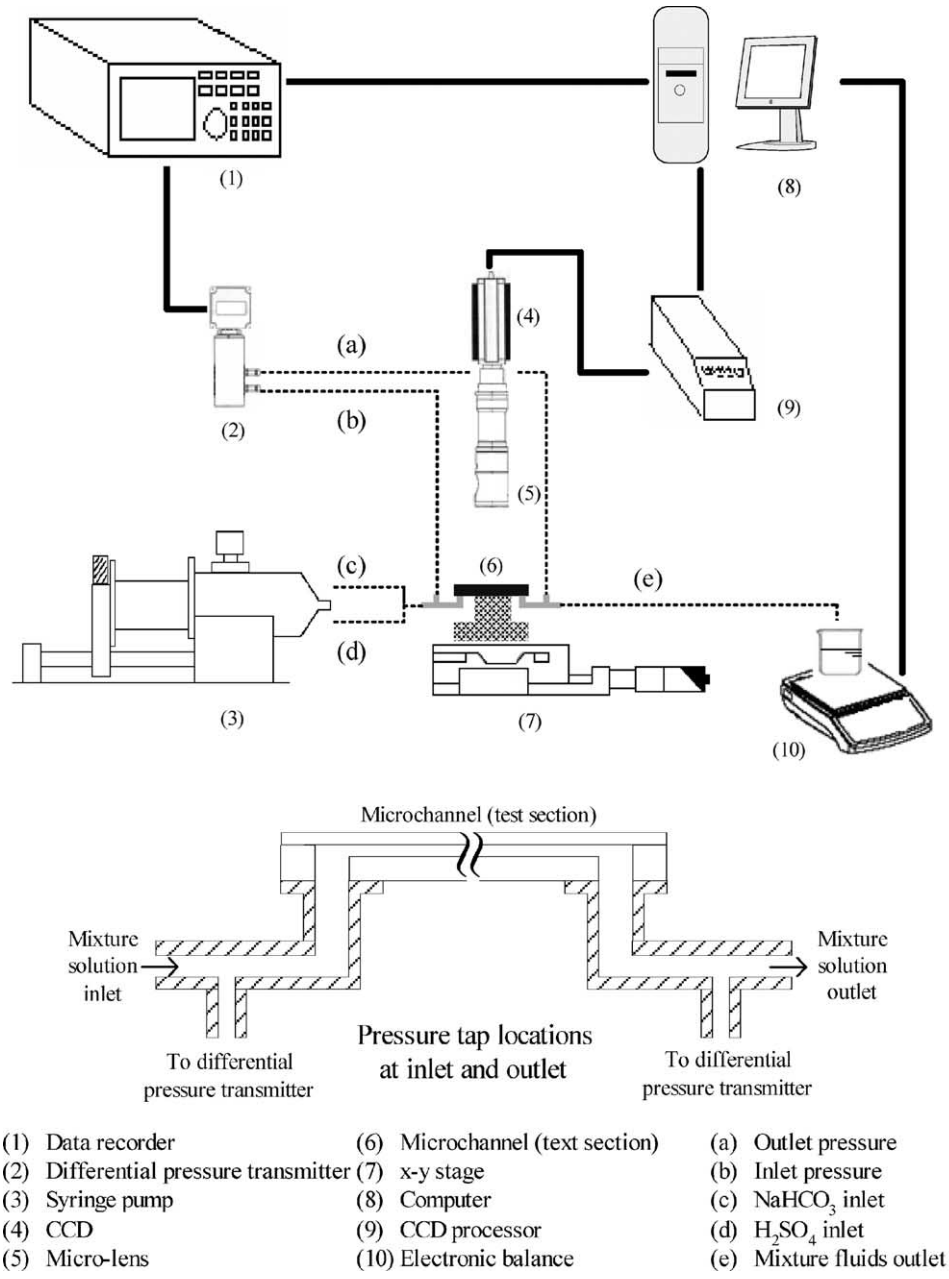

Fig. 1. Experimental apparatus and pressure measurement layout.

cross-section for the connecting tubes is much larger than the test channel, therefore, the pressure loss through the short connecting tubes may be neglected. The differential pressure transducer employed in the present study (Huba 692) is with a short response time of 0.005 s and the sampling rate for pressure drop measurement was set at 100 Hz. Therefore, the high frequency phenomena may be caught. The geometric data of the test section are illustrated in Fig. 2. The channel width and depth were 575 μm and 75 μm, respectively, resulting a hydraulic diameter of 132.7 μm. The length of the channel was 20 mm.

The flow visualization system included a high-speed digital camera (KODAK motion coder SR-ultra), a monitor and a personal computer. To observe the two-phase flow patterns in the microchannel, a microlens was mounted on the CCD. Moreover, an x–y–z mechanism was installed with the test module to hold the lens

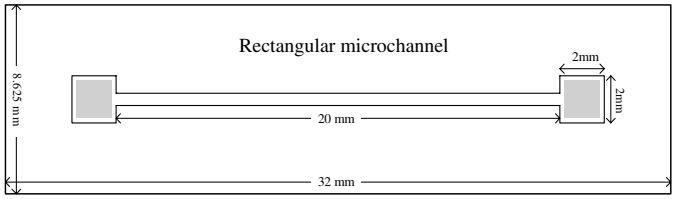

Fig. 2. The geometric data of the microchannel. (■: Excimer laser-etched hole).

and provide accurate position on the test plane (x–y plane) and focusing (z-direction).

2.2. Fabrication of the test section

The test section was a $8.625\,\text{mm} \times 32\,\text{mm}$ silicon stripe, which was made of P-type $\langle 1\,0\,0 \rangle$ orientation wafer. The fabrication process of the microchannel employed bulk micromachining and anodic bonding process. The microchannel and mixing regions, at the inlet and the exit, before and after the channel, were etched by using deep reactive ion etching. Subsequently, the direct writing of excimer laser micromachining technology was applied for the through hole under the mixing regions. To enable flow visualization, the top surface was covered with Pyrex #7740 glass through anodic bonding.

2.3. Experimental procedure

The present study employed aqueous solutions of sulfuric acid (H_2SO_4) and sodium bicarbonate ($NaHCO_3$) as the working fluids. Both reactant solutions were driven by a syringe pump at the same flow rate. The volume flow rates for both solutions were set the same and ranged from $1.60 \times 10^{-9}\,\text{m}^3/\text{s}$ to $16.0 \times 10^{-9}\,\text{m}^3/\text{s}$. Three concentrations of both reactants at the inlet before mixing, C, of 0.2, 0.5 and 0.8 mol/L were investigated. The employment of the same concentration for both reactants at the inlet might consume thoroughly sodium bicarbonate in the channel and help the estimation the production rate of CO_2. If sodium bicarbonate were totally consumed, the volume flow rate of CO_2 produced would be 7.69×10^{-9} to $76.9 \times 10^{-9}\,\text{m}^3/\text{s}$, 19.2×10^{-9} to $192 \times 10^{-9}\,\text{m}^3/\text{s}$, 30.8×10^{-9} to $308 \times 10^{-9}\,\text{m}^3/\text{s}$, respectively, corresponding to $C = 0.2$, 0.5 and 0.8 mol/L depending on flow rate. The evolution of two-phase flow patterns in the microchannel was visualized employing the high speed video camera. The typical frame rate used was 500 frames/s and the exposure time was 1/20,000 s. A 250 W fiber optic illuminator was used as the light source.

2.4. Measurement uncertainty

The measurement uncertainty for flow rate in the microchannel after calibration was estimated to be 0.54%. The measurement uncertainty of pressure transducer was 0.5%.

3. Results and discussion

3.1. Two-phase flow pattern

The flow rate and concentrations of reactants at the inlet have a significant effect on the evolution of two-phase flow pattern in the microchannel. Figs. 3–6 illustrate the effects of flow rate on the development of two-phase flow patterns for both reactants at the inlet with a concentration before mixing, C, of 0.2, 0.5 and 0.8 mol/L, respectively. In these figures, the regions 1 and 4 stand for the region right after the inlet and the region just before the exit, respectively, as clearly shown in the figure. On the other hand, the regions 2 and 3 are for that at one third and two thirds from the inlet, respectively.

For $C = 0.2$ mol/L, no bubbles are produced in the microchannel for flow rates, $Q_H = Q_N \geqq 11.2 \times 10^{-9}\,\text{m}^3/\text{s}$. The Reynolds number corresponding to these flow rates are from 66.9 to 95.5 and flow in the channel is expected to be laminar and poor mixing for both solutions. On the other hand, the flow speeds for both fluids are relatively large for these cases with mean value ranging from 0.519 to 0.741 m/s. Such relatively short duration time for both reactants in the channel may prevent chemical reaction from occurring and, therefore, bubble formation in the microchannel. Fig. 3, however, shows that CO_2 bubbles are formed in the exit reservoir possibly due to mixing effect and flow retardation there.

For $Q_H = Q_N = 9.60 \times 10^{-9}\,\text{m}^3/\text{s}$, a nearly spherical bubble appears in the channel and becomes larger and larger while it travels downstream. Slug flow with elongated bubble appears if the flow rate is reduced to $Q_H = Q_N = 8.00 \times 10^{-9}\,\text{m}^3/\text{s}$. Slug flow prevails in the whole channel as the flow rate is smaller than or equal to $6.40 \times 10^{-9}\,\text{m}^3/\text{s}$. It appears that at these low flow rates bubbles are already generated in the inlet reservoir, indicating the mixing effect there, and the bubble becomes longer and longer while it flows downstream. Moreover, small spherical bubbles may be formed in the middle of the channel accompany the large bubble slug.

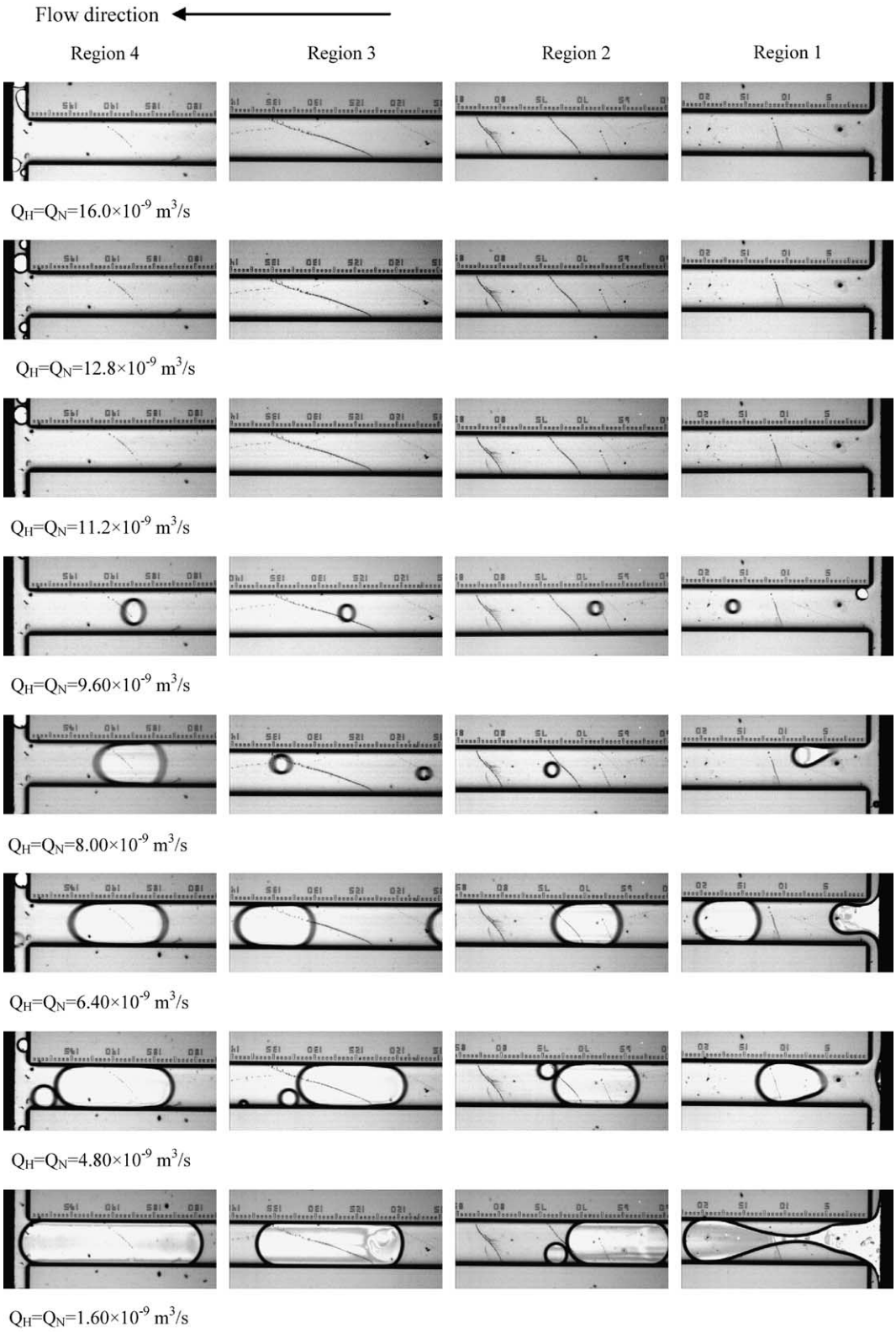

Fig. 3. Effect of reactants' flow rates on the evolution of two-phase flow pattern, $C = 0.2$ mol/L. Dark bands at the inlet and outlet are part of the inlet and outlet reservoir.

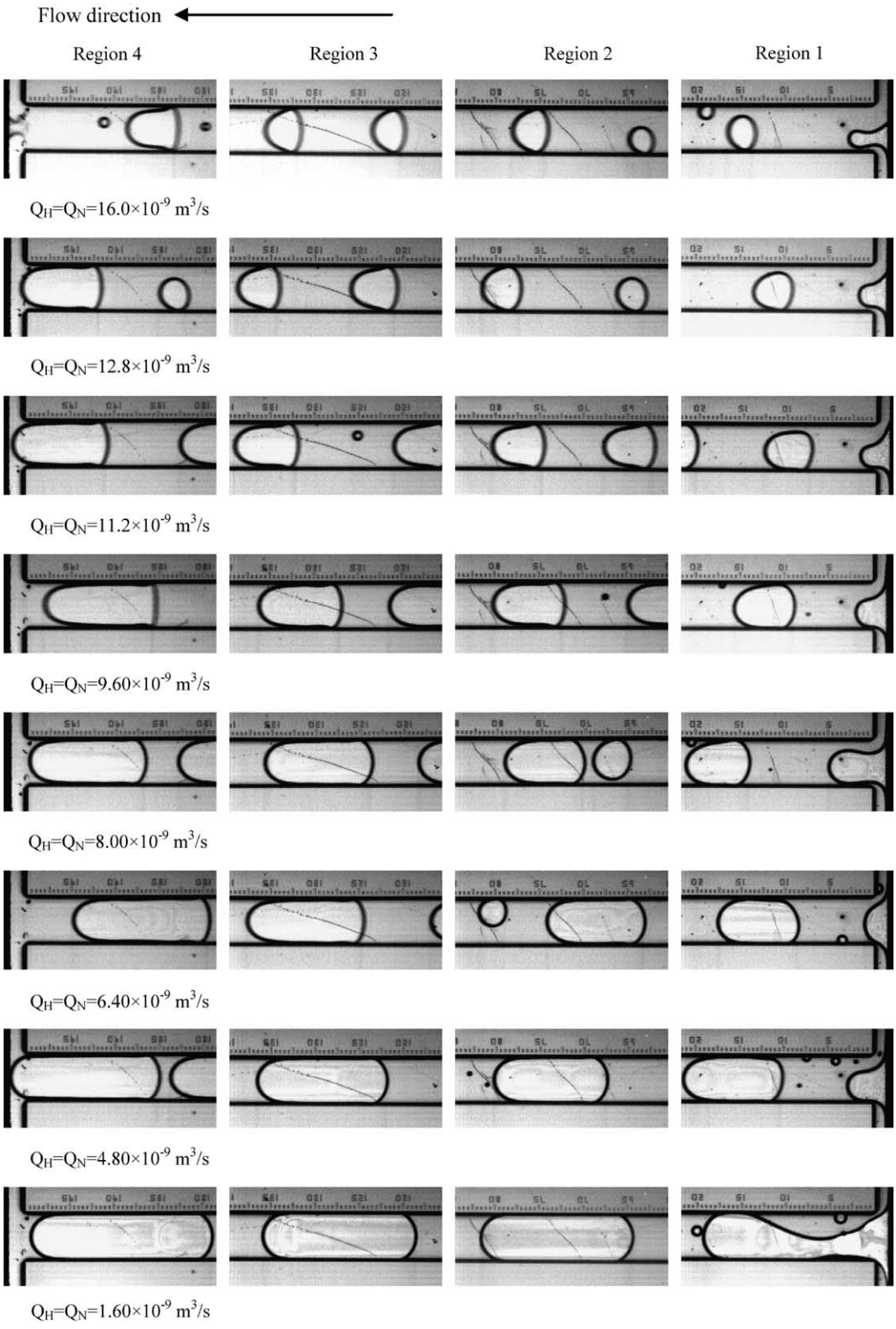

Fig. 4. Effect of reactants' flow rates on the evolution of two-phase flow pattern, $C = 0.5$ mol/L.

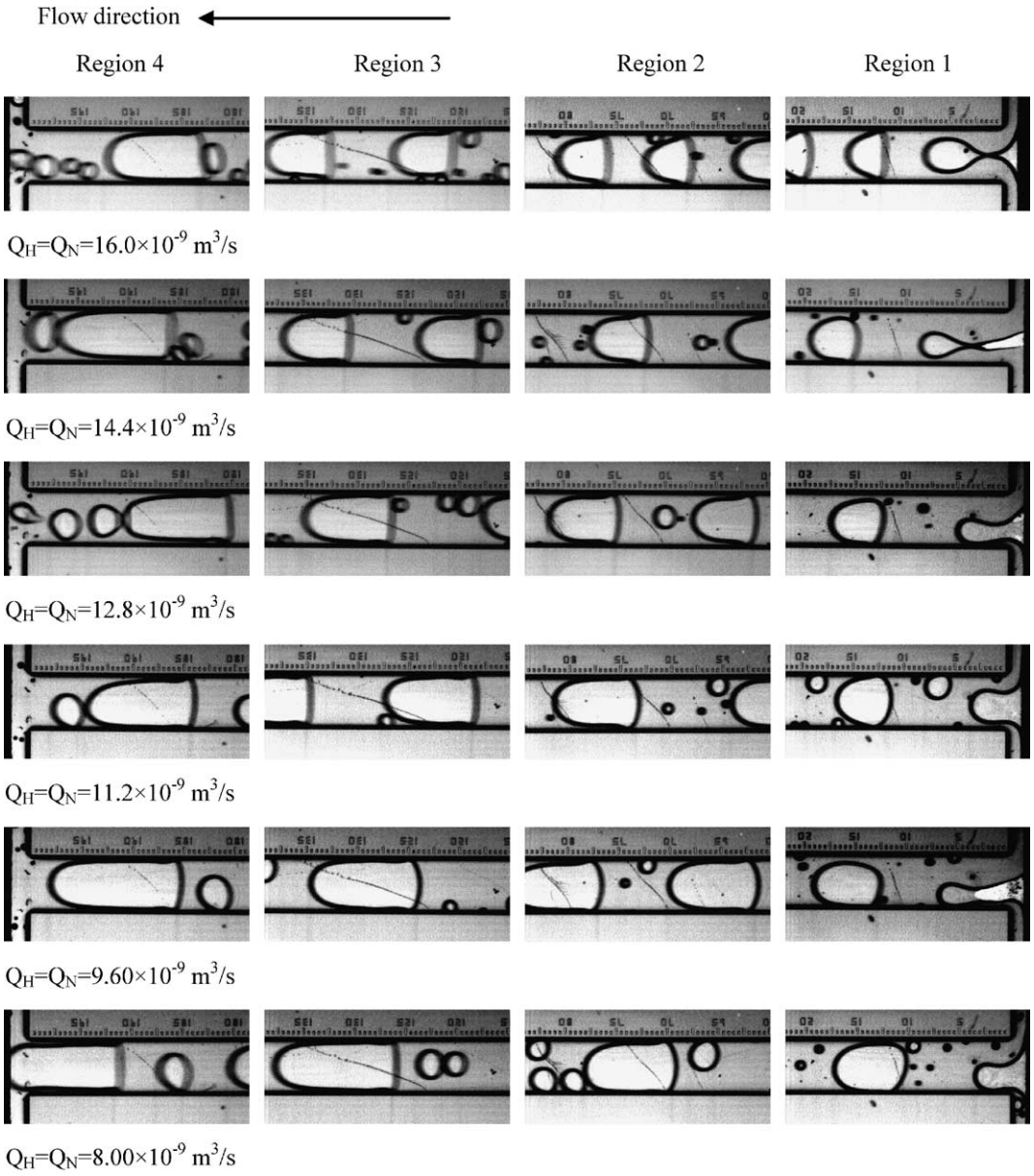

Fig. 5. Effect of reactants' flow rates on the evolution of two-phase flow pattern, $C = 0.8$ mol/L, without flow pattern transition oscillation.

Fig. 4 displays the effects of flow rate on the evolution of two-phase flow pattern in the microchannel for $C = 0.5$ mol/L. For such a middle high inlet concentration, slug flow prevails in the whole channel in the range of flow rates investigated in this work except for the region 1 at the highest flow rate. Bubbles are generated in the inlet reservoir and become longer and longer while it flows downstream due to more CO_2 produced. Small to medium spherical bubbles may also be formed. The bubble length near the channel exit increases with decreasing the flow rate.

The effects of flow rate on the development of two-phase flow pattern in the microchannel for $C =$ 0.8 mol/L are demonstrated in Figs. 5 and 6. For such a high inlet concentration, the flow pattern is characterized by slug flow with small bubbles present between two bubble slugs. Moreover, for 16.0×10^{-9} m^3/s $\geqq Q_H = Q_N \geqq 8.00\times10^{-9}$ m^3/s, the two-phase flow is relatively stable, while the two-phase flow pattern and pressure drop are oscillating for $Q_H = Q_N \leqq 6.40\times10^{-9}$ m^3/s. For such low flow rates, the flow pattern alternates from bubbly-slug flow to slug flow as shown in Fig. 6. The

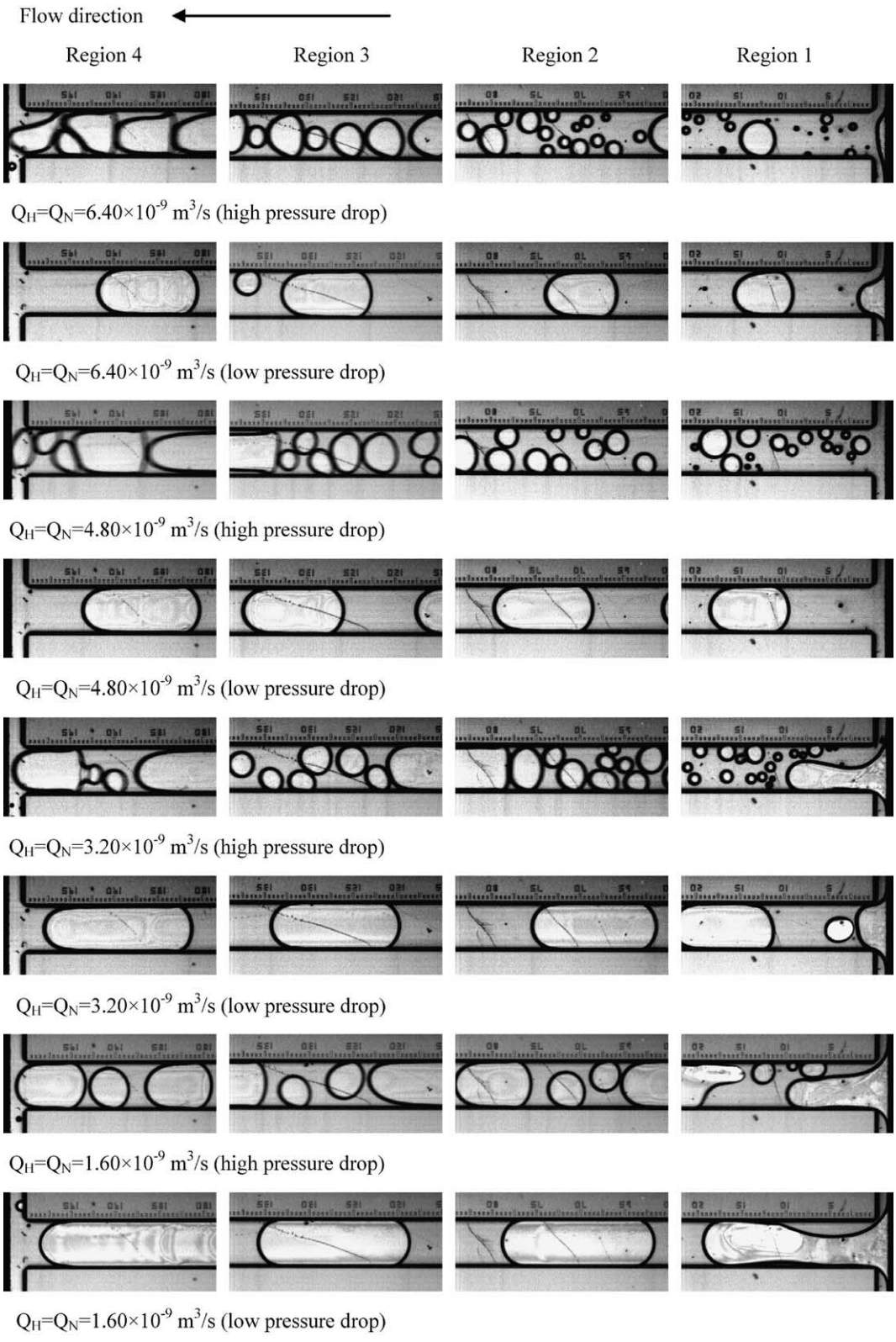

Fig. 6. Effect of reactants' flow rates on the evolution of two-phase flow pattern, $C = 0.8$ mol/L, with flow pattern transition oscillations.

former is characterized by the presence of many small to medium bubbles in the liquid slug, while almost only elongated bubbles are present for the later. The bubbly-slug flow is corresponding to high pressure drop, while the slug flow appears with low pressure drop. Further investigation and discussion will be provided in the following section.

3.2. Pressure drop

Fig. 7 illustrates the total pressure drop, from inlet reservoir to outlet reservoir, as a function of flow rate for three inlet concentrations. In general, the pressure drop increases with increasing the flow rate as well as the inlet concentration. The increase of pressure drop due to flow rate is basically hydrodynamic, while the increasing effect of concentration is caused by the increasing void fraction of CO_2 at high concentrations.

As discussed in the previous section, for $C = 0.2$ mol/L and $Q_H = Q_N \geqq 11.2 \times 10^{-9}$ m^3/s, no bubbles are present in the channel and single-phase flow prevails in the channel. The dash line in the figure shows the pressure drop based on the theoretical predictions as follows:

$$\Delta P_{\text{total}} = \Delta P_{\text{f}} + \Delta P_{\text{in}} + \Delta P_{\text{ex}} \tag{2}$$

where ΔP_{f} stands for the frictional pressure drop and may be evaluated by the Hagen–Poiseuille equation as

$$\Delta P_{\text{f}} = \frac{1}{2}\rho V^2 f \frac{L}{D_{\text{H}}} \tag{3}$$

where f is the friction factor. As discussed previously, the Reynolds number for these cases range from 66.9 to 95.5, laminar flow prevails in the channel. For the present rectangular channel, the friction factor may be evaluated by the following equation [10]:

$$f = \frac{96(1 - 1.3553\gamma + 1.9467\gamma^2 - 1.7012\gamma^3 + 0.9564\gamma^4 - 0.2537\gamma^5)}{Re} \tag{4}$$

where γ is the aspect ratio of the depth to the width of the channel. The Reynolds number in above equation is evaluated based on the mixture density and viscosity of H_2SO_4 and $NaHCO_3$ using the following equation [11]:

$$\rho_{\text{mix}} = \rho_H \cdot x_{H,\text{volume}} + \rho_N \cdot x_{N,\text{volume}} \tag{5}$$

$$\mu_{\text{mix}} = (\mu_H^{1/3} \cdot x_{H,\text{mole}} + \mu_{\text{N}}^{1/3} \cdot x_{N,\text{mole}})^3 \tag{6}$$

In Eq. (2), ΔP_{in} and ΔP_{ex} represent the pressure loss at the inlet and outlet due to sudden contraction and expansion, respectively, and may be evaluated by the following equation:

$$\Delta P_{\text{loss}} = k\frac{1}{2}\rho_L V^2, \tag{7}$$

where k is a loss coefficient based on the velocity head (V) in the small channel [12]

$$k = \begin{cases} [1 - A_{12}]^2, & \text{sudden expansion} \\ 0.42[1 - A_{12}], & \text{sudden contraction} \end{cases} \tag{8}$$

where

$$A_{12} = A_1/A_2, \tag{9}$$

A_1 is the cross-sectional area just before the expansion or after the contraction, and A_2 is the cross-sectional area just before the contraction or after the expansion.

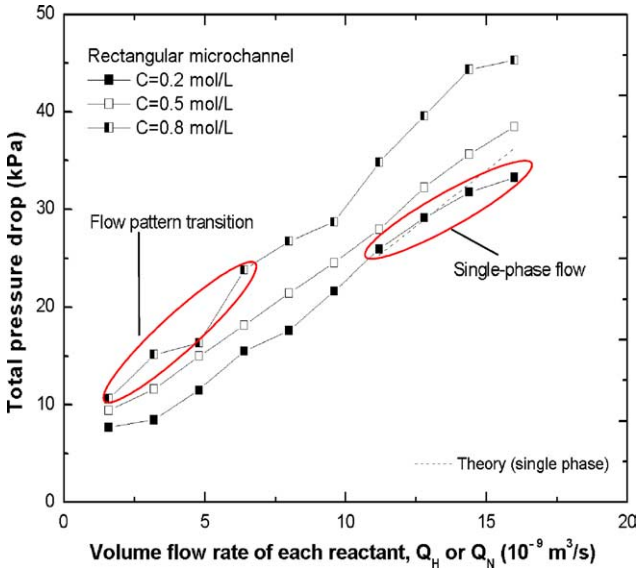

Fig. 7. Total pressure drop as a function of flow rate for different concentrations of reactants at the inlet.

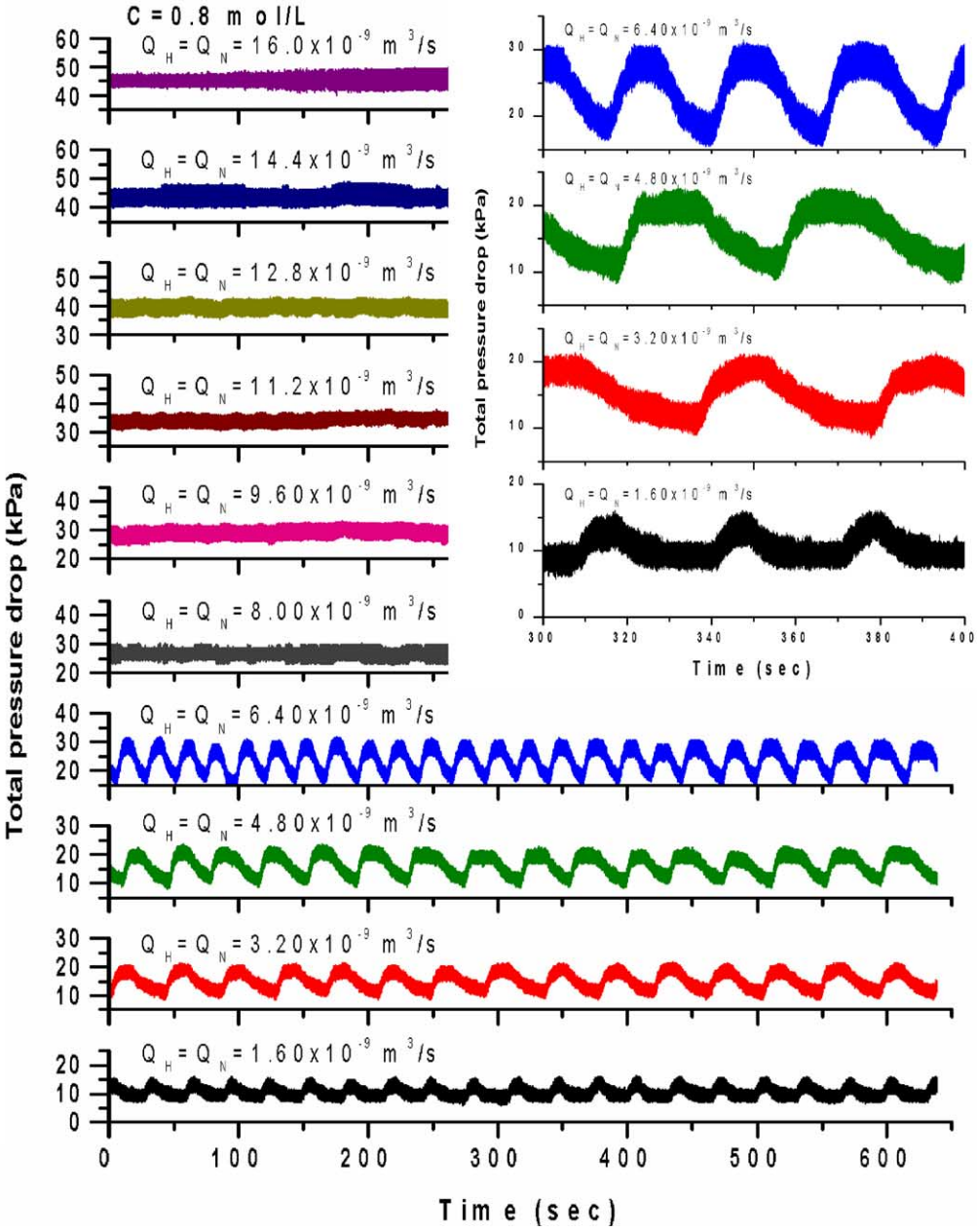

Fig. 8. Pressure drop oscillations at various flow rate for $C = 0.8$ mol/L.

Fig. 7 indicates that for single phase flow the deviation between the theory and experimental data is within 10%, the deviation increases with increasing the flow rate because the data tend to droop at high flow rates.

3.3. Flow pattern transition instability

The flow pattern transition instability between bubbly-slug and slug flow appears for the case of $C = 0.8$ mol/L and $Q_H = Q_N \leqq 6.40 \times 10^{-9}$ m^3/s, as discussed earlier. For these cases the data shown in Fig. 7 are the mean value. The time evolutions of the total pressure drop for various flow rates for this particular inlet concentration are exhibited in Fig. 8. The figure clearly demonstrates large magnitude pressure drop oscillations for $Q_H = Q_N \leqq 6.40 \times 10^{-9}$ m^3/s. The insert magnifies the oscillation pattern for the four cases with flow pattern transition instability. The frequency and magnitude of oscillations for cases with flow pattern instability are displayed in Table 1. The oscillation

Table 1
Pressure drop oscillation frequency, $C = 0.8$ mol/L

Volume flow rate, $Q_H = Q_N$, (10^{-9} m^3/s)	1.60	3.20	4.80	6.40	8.00
Flow pattern transition oscillation frequency (Hz)	0.032	0.024	0.024	0.041	–
Frequency of the modulating envelope (Hz)	7.53	6.15	6.75	7.81	8.40
High-frequency oscillation frequency (Hz)	46.5	46.9	47.0	46.4	45.9
	9.60	11.2	12.8	14.4	16.0
Flow pattern transition oscillation frequency (Hz)	–	–	–	–	–
Frequency of the modulating envelope (Hz)	8.53	8.77	9.08	10.1	–
High-frequency oscillation frequency (Hz)	45.9	45.9	45.5	45.1	42.9

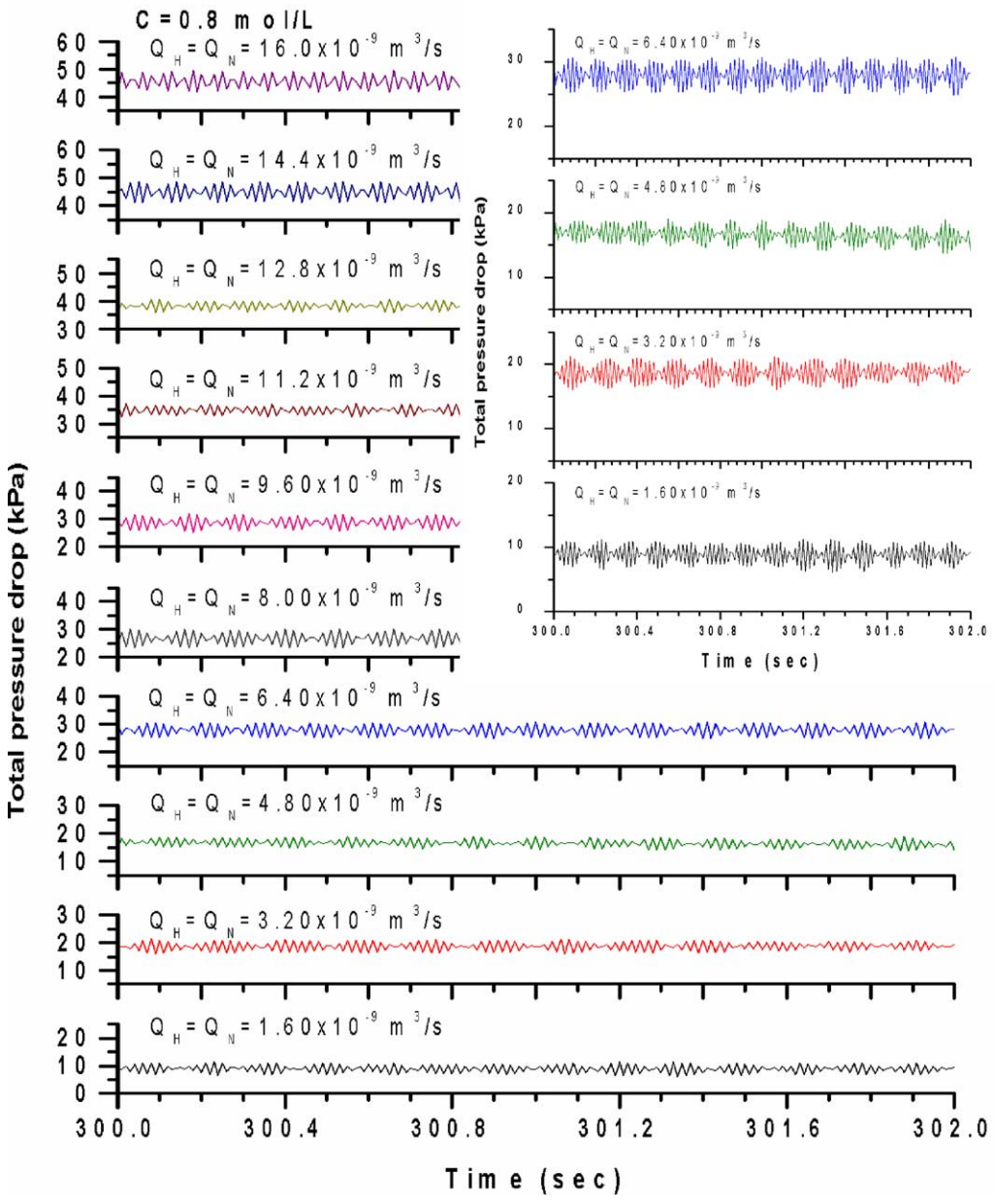

Fig. 9. A detailed view of pressure drop oscillation at various flow rates for $C = 0.8$ mol/L.

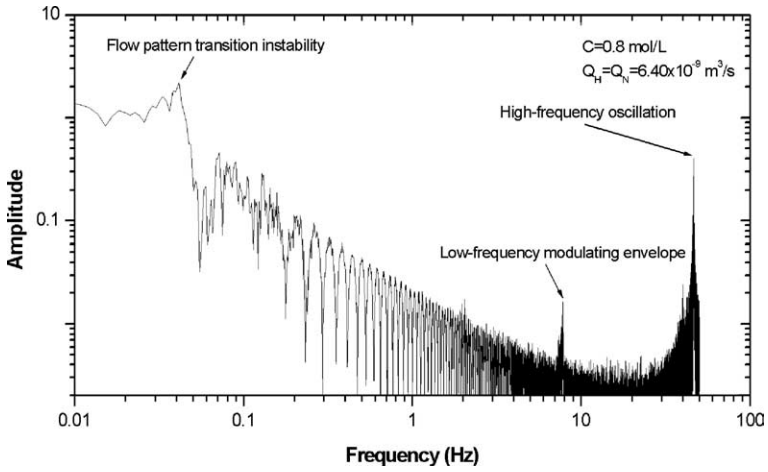

Fig. 10. The frequency spectrum of the pressure drop. ($C = 0.8$ mol/L, $Q_H = Q_N = 6.40 \times 10^{-9}$ m^3/s).

frequency is from 0.024 to 0.041 Hz and the magnitude of oscillation is from 10 to 15 kPa. There seems to have no general trend of flow rate on the oscillation characteristics. As discussed earlier, the peak pressure drop is corresponding to the bubbly flow and the valley one is associated with the slug flow. The oscillation magnitude is the largest for the case of $Q_H = Q_N = 6.40 \times 10^{-9}$ m^3/s because the difference in flow pattern is most distinctive from bubbly-slug to slug flow among the four cases. On the other hand, the oscillation magnitude is the least for the lowest flow rate of this work, i.e., $Q_H = Q_N = 1.60 \times 10^{-9}$ m^3/s as the flow pattern between the two extremes are quite similar. Both are slug flow in essence (see Fig. 6). This suggests that the flow pattern instability appears only in a certain range of flow rate at a given inlet concentration.

Although the flow pattern transition instability has been well-known, the primary mechanism for such instability in a microchannel with chemical reactions is still unexplored in the literature. Moreover, the flow rate for each case remained constant but the inlet pressure and thus the pressure drop was allowed to vary during the experiment. The mechanism for the flow pattern transition instability of the present work is as follows. During the low pressure period, slug flow with elongated bubbles prevails in the channel. For such flow pattern, Thulasidas et al. [13] had demonstrated the existence of flow circulation in the liquid slug with forward flow in the central region and reversed flow in the near wall region. Such a circulation flow in the liquid slug would enhance mixing and, therefore, chemical reaction producing many CO_2 bubbles as shown in Fig. 7. The pressure drop and inlet pressure are, thus, increased due to the presence of these small bubbles. The formation of small bubbles in the liquid slug may eliminate the flow circulation and further chemical reactions on the one hand and increase the collision frequency of bubbles on the other hand. Moreover the high pressure would also force the bubbles to collide and merge. As a result, slug flow is resumed again and another cycle repeats.

3.4. High frequency oscillations

High frequency oscillations are superimposed on the pressure drop data for those cases with the low frequency flow pattern transition instability as well as those cases without, as shown in Fig. 9. The inset illustrates a magnified view of the four cases with flow pattern transition instability. Such high frequency oscillations also prevail for the cases with $C = 0.2$ or 0.5 mol/L. Fig. 10 illustrates the frequency spectrum of the pressure drop data for $C = 0.8$ mol/L and $Q_H = Q_N = 6.40 \times 10^{-9}$ m^3/s through the fast Fourier transformation. The figure clearly demonstrates three distinctive peaks: one at 0.041 Hz corresponding to the low frequency flow pattern transition instability and the other one at 46.4 Hz corresponding to the high frequency oscillations and the other one at 7.81 Hz corresponding to the modulate envelope of the high frequency oscillation. Table 1 lists the numerical values of these three distinguished frequencies for various cases of $C = 0.8$ mol/L. The frequency for these high frequency oscillations ranges from 42.9 to 47.0 Hz, while the frequency of their modulating envelopes is from 6.15 to 10.1 Hz. There seems to be no general trend of flow rate on these two frequencies. The magnitude of such high frequency oscillations is about 5 kPa. Such high frequency oscillations seem to be a kind of acoustic oscillations [5].

4. Summary and conclusions

The present study investigates experimentally the two-phase flow in a microchannel with CO_2 bubbles

generated by chemical reactions of sulfuric acid (H_2SO_4) and sodium bicarbonate ($NaHCO_3$). The following conclusions may be drawn from the results of this study.

1. The concentrations of both reactants at the inlet and flow rate of reactants have significant effects on the evolution of two-phase flow pattern in the microchannel. At the lowest inlet concentration of the present study and high flow rates, no bubbles are formed and single-phase flow prevails in the microchannel. The CO_2 bubbles are produced and the two-phase flow pattern evolves to bubbly or slug flow as the inlet concentration is increased and/or flow rate is reduced. The slug flow is the dominant flow pattern.
2. The flow pattern transition instability between bubbly-slug flow and slug flow takes place for the cases with the highest inlet concentration, i.e., $C = 0.8$ mol/L, and low flow rates. The oscillation frequency is from 0.024 to 0.041 Hz and the magnitude of oscillation is from 10 to 15 kPa.
3. The single phase frictional pressure drop through the microchannel may be predicted using the Hagen–Poiseuille equation with the friction factor evaluated based on a rectangular channel with a given aspect ratio within 10%.
4. The two-phase pressure drop increases with increase in the flow rate as well as the inlet concentration due to more active chemical reactions and, therefore, producing more CO_2 bubbles at high concentrations.
5. The low frequency flow pattern transition instability is superimposed with high frequency oscillations with a frequency of about 46–47 Hz. Such high frequency oscillations also prevail for other cases without flow pattern transition.

Acknowledgement

This work was supported by the National Science Council of Taiwan under the contract no. of NSC 92-2212-E-007-093.

References

[1] P. Argyropulos, K. Scott, W.M. Taama, Gas evolution and power performance in direct methanol fuel cells, J. Appl. Electrochem. 29 (1999) 661–669.
[2] P.C. Lee, F.G. Tseng, C. Pan, Bubble dynamics in microchannels. Part I. Single microchannel, Int. J. Heat Mass Transfer 47 (2004) 5575–5589.
[3] J.J. Hwang, F.G. Tseng, C. Pan, Ethanol-CO_2 two-phase flow in diverging and converging microchannels, Int. J. Multiphase Flow 31 (2005) 548–570.
[4] D.S. Meng, J. Kim, C.J. Kim, A distributed gas breather for micro direct methanol fuel cells (μ-DMFC), in: Proceedings of the IEEE Int. Conf. on Micro Electro Mechanical Systems (MEMS'03), Kyoto, Japan, January 19–23, 2003, pp. 534–537.
[5] J.A. Boure, A.E. Bergles, L.S. Tong, Review of two-phase flow instability, Nucl. Eng. Des. 25 (1973) 165–192.
[6] H.Y. Li, P.C. Lee, F.G. Tseng, C. Pan, Two-phase flow instability of boiling in a double microchannel system at high heating powers, in: Proc. First Int. Conf. on Microchannels and Minichannels, Rochester, New York, USA, April 24–25, 2003, pp. 615–622.
[7] H.Y. Wu, P. Cheng, Visualization and measurements of periodic boiling in silicon microchannels, Int. J. Heat Mass Transfer 46 (2003) 2603–2614.
[8] W. Qu, I. Mudawar, Measurement and prediction of pressure drop in two-phase micro-channel heat sinks, Int. J. Heat Mass Transfer 46 (2003) 2737–2753.
[9] R.T. Lahey Jr., M.Z. Podowski, On the analysis of various instabilities in two-phase flows, in: G.F. Hewitt, J.M. Delhaye, N. Zuber (Eds.), Multiphase Science and Technology, vol. 4, Hemisphere Publishing Co, New York, 1989 (Chapter 3).
[10] J.P. Hartnett, M. Kostic, Heat transfer to Newtonian and non-Newtonian fluids in rectangular ducts, Adv. Heat Transfer 19 (1989) 247–356.
[11] J. Kendall, K.P. Monroe, The viscosity of liquids II. The viscosity-composition curve for ideal liquid mixtures, J. Am. Chem. Soc. 39 (1917) 1787–1802.
[12] F.M. White, Fluid Mechanics, McGraw-Hill Book Co., New York, 1979, p. 356.
[13] T.C. Thulasidas, M.A. Abraham, R.L. Cerro, Bubble-train flow in capillaries of circular and square cross-section, Chem. Eng. Sci. 50 (1995) 183–199.